Supporting Information

Experimental and Theoretical Evidence for an Unusual Almost Triply Degenerate Electronic Ground State of Ferrous Tetraphenylporphyrin

Maxime Tarrago,[†] Christina Römelt,[‡] Joscha Nehrkorn,[‡] Alexander Schnegg,[‡] Frank Neese*[,†] Eckhard Bill,*[,‡] and Shengfa Ye*[,†,§]

[†]Max-Planck-Institut für Kohlenforschung, Kaiser-Wilhelm-Platz 1, D-45470 Mülheim an der Ruhr, Germany

[‡]Max-Planck-Institut für Chemische Energiekonversion, Stiftstr. 34-36, D-45470 Mülheim an der Ruhr, Germany

[§]State Key Laboratory of Catalysis, Dalian Institute of Chemical Physics, Chinese Academy of Sciences, Dalian 116023, China

Table of Contents

Table S1: Computed relative energies of the low-lying triplet states of four-coordinated iron-porphyrins in the literature (in cm^{-1}):

Method	$\Delta_{A\text{-}E} = E(^3E_g(A)) - E(^3A_{2g})$
Configuration Interaction	-3791[1]
Stochastic CASSCF	-175[2]
MRPT	-1847[3]
CASSCF/CASPT2	145[4]
CASSCF/CASPT2	804[5]
CCSD(T)	595[6]
DLPNO-CCSD(T)	689[7]

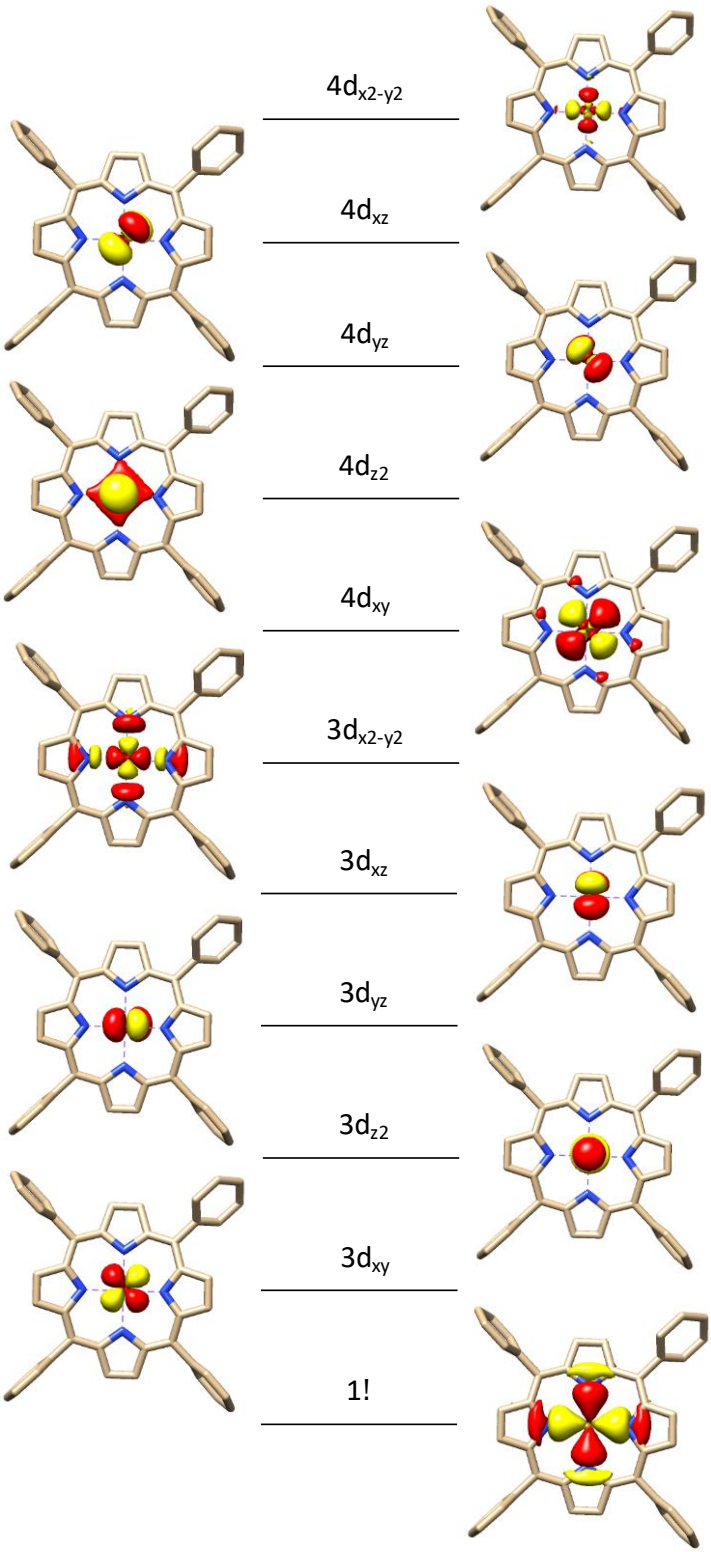

Figure S1: Active space CAS(8,11) for **1** (ruffled conformation). The active space is composed of the valence d-shell (3d), the double d-shell (4d), plus the σ-bonding counterpart of the $3d_{x2-y2}$ orbital (1σ). The same active space was used for **1** in saddle conformation and [Fe(TTP)] in planar conformation. For clarity, hydrogens are omitted.

Carbons are displayed in beige, nitrogens in blue and iron in orange. Negative and positive parts of the orbitals are represented as yellow and red isosurfaces.

Electronic Spin Hamiltonian

The electronic spin Hamiltonian is here expressed in the basis of the three $\tilde{S}$ =1 pseudospin eigenstates ($M_{\tilde{S}} = 0, \pm 1$). It includes the zero-field splitting (H_{ZFS}) and Zeeman effect ($H_{\mathrm{Zee,SH}}$), described as follows:

$$\hat{H} = H_{\mathrm{ZFS}} + H_{\mathrm{Zee,SH}} = \vec{\tilde{S}} \cdot \bar{\bar{D}} \cdot \vec{\tilde{S}} + \mu_{\mathrm{B}} \overrightarrow{B_{\mathrm{ext}}} \cdot g \cdot \vec{\tilde{S}} \quad \text{(S1)}$$

Where $\vec{\tilde{S}}$ is the pseudospin operator, $\bar{\bar{D}}$ the zero-field splitting tensor, μ_B the Bohr magneton, $\overrightarrow{B_{\mathrm{ext}}}$ is the applied field and g the g-matrix. $\bar{\bar{D}}$ and g have the same principal axis system dictated by the high symmetry of the molecule. The z-component is along the C_4 rotation axis, and the x and y components lie anywhere on the porphyrin plane. This enables the use of a unique set of x,y,z axes in which both g and $\bar{\bar{D}}$ are diagonal. Were this not the case, additional parameters corresponding to the rotation transformation from one principal coordinate system to another would be required. In the main text, the components of the D tensor are expressed as:

$$D = \frac{3}{2} D_{\mathrm{ZZ}} \quad \text{(S1a)}$$

$$E = \frac{D_{\mathrm{XX}} - D_{\mathrm{yy}}}{2} \quad \text{(S1b)}$$

The components of the g-matrix are re-expressed into $g_\perp = g_{xx} = g_{yy}$ as constrained by the molecular symmetry and $g_\parallel = g_{zz}$. The spin Hamiltonian is re-expressed as:

$$\hat{H} = D\left[\hat{\tilde{S}}_z^2 - \frac{1}{3}\tilde{S}(\tilde{S}+1) + \frac{E}{D}\left(\hat{\tilde{S}}_x^2 - \tilde{S}_y^2\right)\right] + \mu_{\mathrm{B}} \overrightarrow{B_{\mathrm{ext}}} \cdot \bar{\bar{g}} \cdot \tilde{S} \quad \text{(S1c)}$$

Where $\tilde{S}$ is the pseudospin quantum number, $\tilde{S}_{\mathrm{x}}$, $\tilde{S}_{\mathrm{y}}$ and $\tilde{S}_{\mathrm{z}}$ are the components of the pseudospin operator.

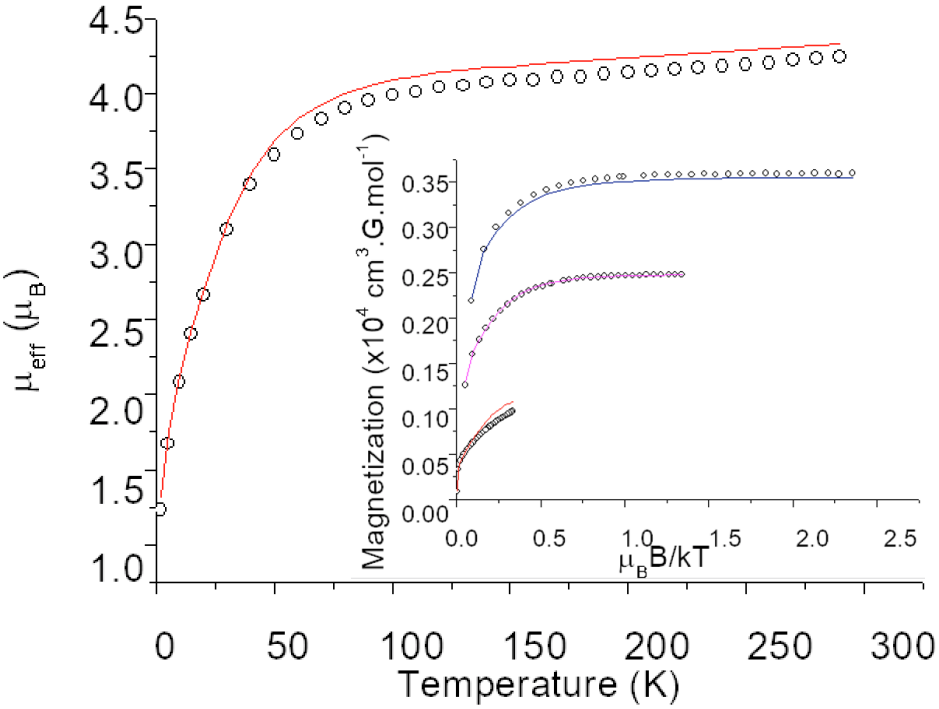

Figure S2: Effective magnetic moment of a powder sample of **1** recorded with a field of 1 T, and temperature dependence of the magnetization with applied fields of 1 (red), 4 (magenta) and 7 T (blue) (inset). The solid lines represent the best fits obtained by the simulation using the spin Hamiltonian (parameters g_{xx}=g_{yy}= 3.07, g_{zz}=1.7, D=94 cm^{-1}, $\frac{E}{D}$ = 0, χ_{TIP} = 1000 × 10^{-6} emu). **The simulation takes into account 5.5% S = 5/2 impurity**, instead of the 7.9% S=2 impurities in Figure 1 of the main text.

THz-EPR

Experiments were performed at the THz beam line of the synchrotron BESSY II, Helmholtz-Zentrum Berlin. The experiment is described elsewhere in great detail.[8] 12 mg of polycrystalline powder of **1** was mixed with PE powder, grinded and pressed into a TPX sample holder. An Hg arc lamp was used for irradiation. Inside the FT-IR spectrometer (IFS 125, Bruker) the radiation was divided by a 6 µm Mylar multilayer beam splitter. Mirror movements corresponded to a scanner velocity of 40 kHz and an experimental resolution of 1 cm^{-1}. The sample was placed in the VTI of an Oxford Optistat magnet with outer TPX and inner diamond windows and kept at a temperature of 5 K. Radiation passed through the magnet (and the sample) in Voigt configuration and was detected with an Infrared 4.2K Si bolometer. At each field, 256 scans were acquired. Spectra are shown as Magnetic field division spectra (MDS), where the spectrum for the field B_0 is obtained by dividing a spectrum measured at B_0 + 1 T by a spectrum measured at B_0 (further details on how to analyze MDS can be found in ref. 8). Simulations were performed with EasySpin[9] and its extensions for frequency-domain EPR.[10] The simulation used the same spin-Hamiltonian defined in Eq. S1c.

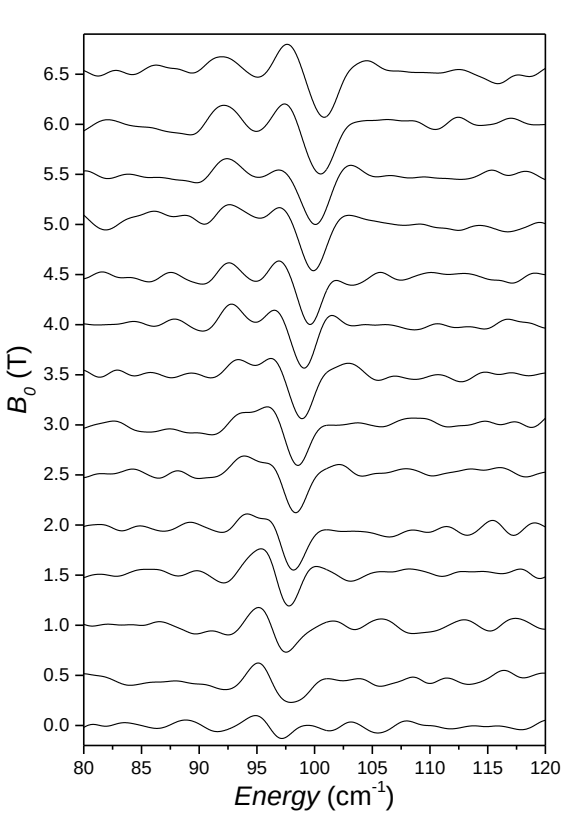
6.5
6.0
5.5
5.0
4.5
4.0
3.5
3.0
2.5
2.0
1.5
1.0
0.5
0.0
B_0 (T)
80
85
90
95
100
105
110
115
120
Energy (cm^{-1})

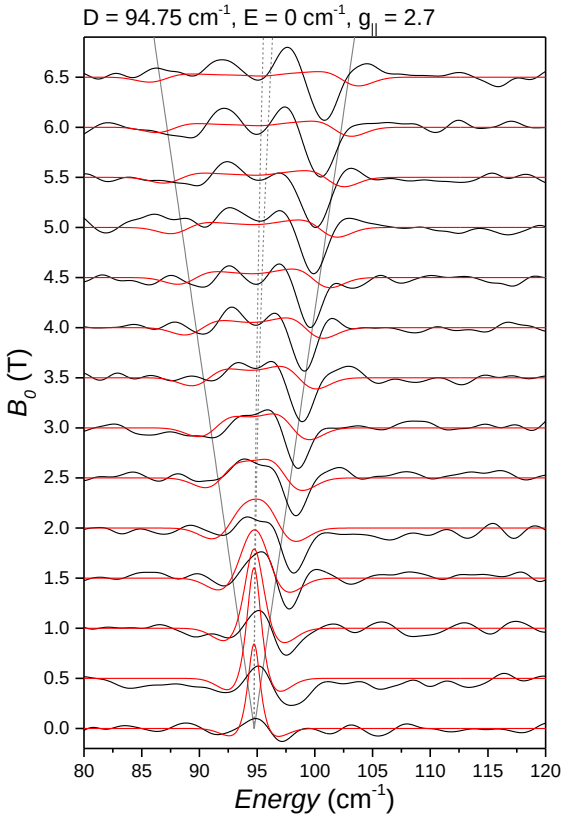
D = 94.75 cm^{-1}, E = 0 cm^{-1}, g$_{||}$ = 2.7
6.5
6.0
5.5
5.0
4.5
4.0
3.5
3.0
2.5
2.0
1.5
1.0
0.5
0.0
B_0 (T)
80
85
90
95
100
105
110
115
120
Energy (cm^{-1})

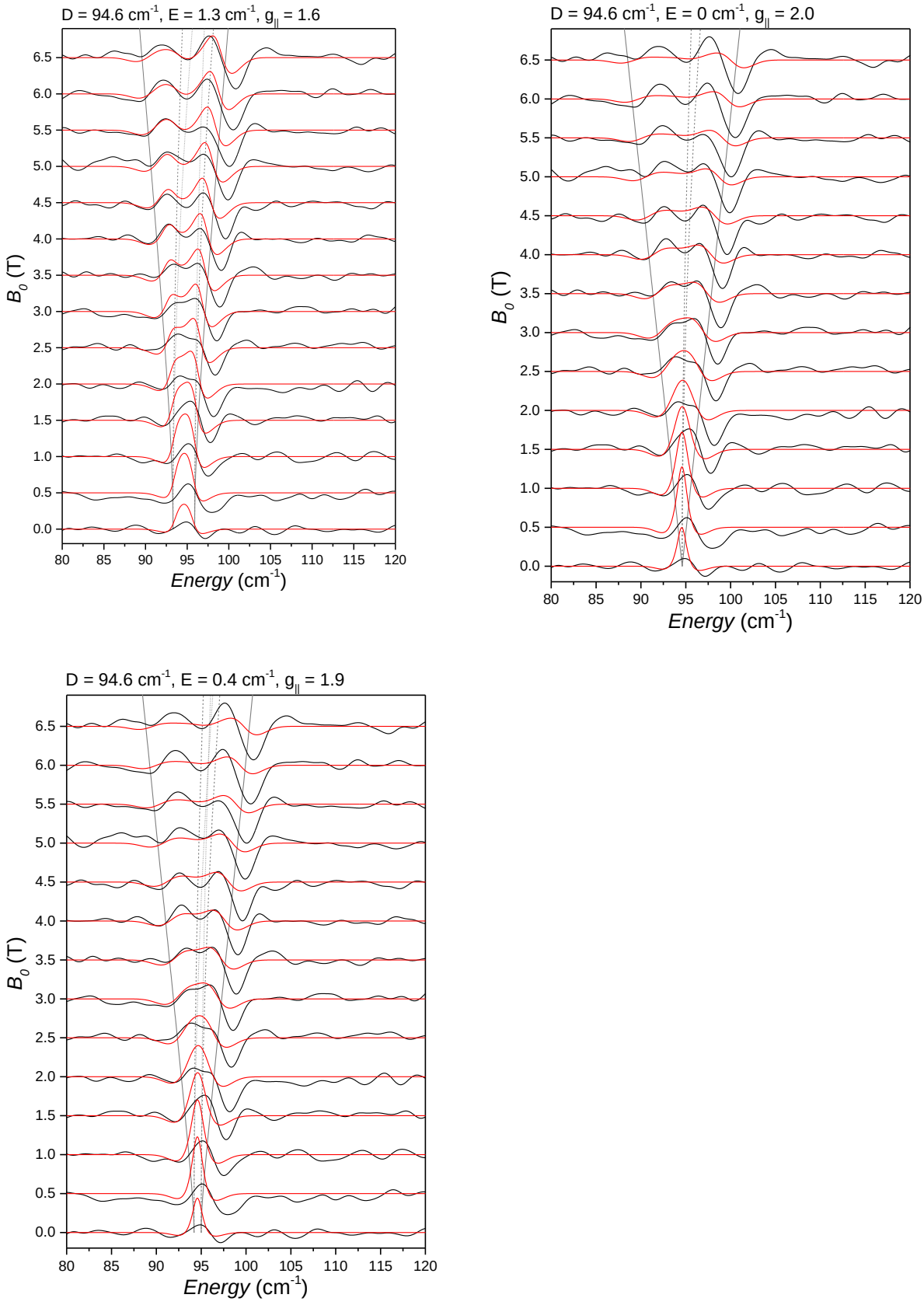

Figure S3: THz-EPR spectra of **1**. Data (black line) is rescaled and offset according to the applied magnetic field B_0. Simulation with the parameters shown on top of each plot are shown

in red. Gray lines in the back indicate calculated transition energies for a magnetic field applied along the x- (dashed), y- (dotted), and z-axis (solid).

Nuclear spin Hamiltonian

As described in the Main Text, the nuclear spin Hamiltonian is constituted of the electric quadrupole interactions ($\mathrm{H}_\delta + H_\mathrm{Q}$), the nuclear Zeeman effect (H_Z), and the magnetic hyperfine coupling effect ($H_\mathrm{HFC,SH}$).

$$H_\mathrm{Nuc,SH} = \mathrm{H}_\delta + H_\mathrm{Q} + H_\mathrm{Z} + H_\mathrm{HFC,SH} \quad \text{(S2)}$$

$$\mathrm{H}_\mathrm{Nuc,SH} = \mathrm{H}_\delta + \frac{eQ}{2I(2I-1)}\left(V_{zz}\hat{I}_z{}^2 + V_{xx}\hat{I}_x{}^2 + V_{yy}\hat{I}_y{}^2\right) - g_N\beta_N\vec{I}\cdot\overrightarrow{B_{ext}} + \vec{I}\cdot A\cdot\vec{\tilde{S}} \quad \text{(S2a)}$$

Where e is the elementary charge of the proton, Q the quadrupole moment of the nucleus (taken as 0.16 Barns), I the nuclear spin quantum number, $\hat{I}_\alpha$ the α-component of the nuclear spin angular momentum operator, $V_{\alpha\alpha}$ the α-component of the electric field gradient tensor (the α component corresponds to x,y or z component), g_N the nuclear g-factor of the ^{57}Fe nucleus (0.181 for the ground state I = 1/2, -0.103 for the excited state I = 3/2), β_N the nuclear magneton, and A the hyperfine coupling matrix. Due to the high symmetry of the molecule, the electric-field gradient tensor and the hyperfine coupling matrices have the same principal axis system as the g-matrix and the D-tensor. As stated above, this enables the description of one unique set of x,y,z axes in which all four matrices are diagonal, thus reducing the required number of fitting parameters (vide supra).

In the main text, the $\mathrm{V}_{\alpha\alpha}$ are expressed indirectly via the quadrupole splitting and η parameters

$$\Delta E_Q = \frac{eQV_{zz}}{2} \quad \text{(S2b)}$$

$$\eta = \frac{V_{xx}-V_{yy}}{V_{zz}} = 0 \quad \text{(S2c)}$$

The hyperfine coupling operator is calculated under the approximation that the nuclear and electronic spins are decoupled. Under this approximation, the electronic pseudospin may be replaced by its expectation value. For variable temperature measurements, the fast electron spin relaxation regime is used. In this regime, the electron spin expectation value is replaced by the Boltzmann average of the spin expectation values for each thermally populated magnetic sublevel. In other words, the hyperfine coupling Hamiltonian becomes:

$$H_{HFC} = \vec{I}\cdot\bar{\bar{A}}\cdot\frac{\sum_i\langle\vec{S}\rangle_i e^{-\frac{E_i}{k_BT}}}{\sum_i e^{-\frac{E_i}{k_BT}}} \quad \text{(S3)}$$

Where i runs over all populated magnetic sublevels $\langle\vec{S}\rangle_i$ is the expectation value of the pseudospin operator vector for the magnetic sublevel i, E_i the energy of the magnetic sublevels i, k_B the Boltzmann constant, and T the temperature.

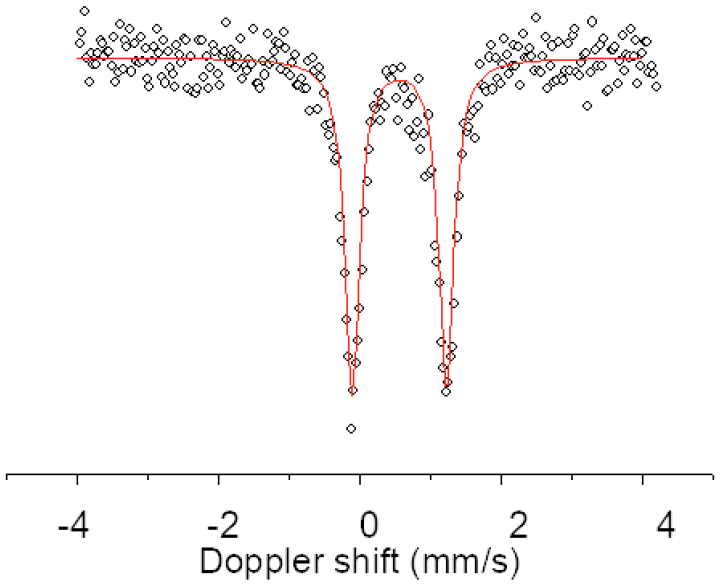

Figure S4: Fit of the ^{57}Fe Mössbauer spectrum at 80 K under no applied field. The dots correspond to the experimental measurements and the red line corresponds to the fit, using the following phenomenological parameters: $|\Delta E_Q| = 1.31$ mm/s and $\delta = +0.56$ mm/s.

State compositions of the Lz eigenstates and symmetry-adapted relativistic states in the D4 point group (after in-state SOC)

L_z eigenstates:

$$\left|{}^3E_g, M_S, +\right\rangle = \frac{1}{\sqrt{2}} \left(\left|{}^3E_g(y), M_S\right\rangle - i \left|{}^3E_g(x), M_S\right\rangle \right) \quad \text{(S4a)}$$

$$\left|{}^3E_g, M_S, -\right\rangle = \frac{1}{\sqrt{2}} \left(\left|{}^3E_g(y), M_S\right\rangle + i \left|{}^3E_g(x), M_S\right\rangle \right) \quad \text{(S4b)}$$

Symmetry-adapted states:

$$\left|{}^3E_g, A_2\right\rangle = \frac{1}{\sqrt{2}} \left(\left|{}^3E_g, +1, -\right\rangle + \left|{}^3E_g, -1, +\right\rangle \right) \quad \text{(S4c)}$$

$$\left|{}^3E_g, A_1\right\rangle = \frac{1}{\sqrt{2}} \left(\left|{}^3E_g, +1, -\right\rangle - \left|{}^3E_g, -1, +\right\rangle \right) \quad \text{(S4d)}$$

$$\left|{}^3E_g, E_\pm\right\rangle = \mp \left|{}^3E_g, 0, \pm\right\rangle \quad \text{(S4e)}$$

$$\left|{}^3E_g, B_2\right\rangle = \frac{1}{\sqrt{2}} \left(\left|{}^3E_g, +1, +\right\rangle + \left|{}^3E_g, -1, -\right\rangle \right) \quad \text{(S4f)}$$

$$\left|{}^3E_g, B_1\right\rangle = \frac{1}{\sqrt{2}} \left(\left|{}^3E_g, +1, +\right\rangle - \left|{}^3E_g, -1, -\right\rangle \right) \quad \text{(S4g)}$$

Inclusion of the quintet state into the model

The model has been extended to include the 5 magnetic sublevels of the $^5A_{1g}$ orbital state with electronic configuration $(d_{z2})^2(d_{xy})^1(d_{x2-y2})^1(d_{xz})^1(d_{yz})^1$ as low as 800 cm^{-1} above the $^3A_{2g}$ orbital state. This number corresponds to the energy difference between those states calculated via CASSCF/NEVPT2 for the ruffled core-conformation of **1**. The representation of a S = 2 spin function in the D_4 group is given according to the following rule:

$$\chi^S(\phi) = \frac{\sin\left(S+\frac{1}{2}\right)\phi}{\sin\left(\frac{1}{2}\phi\right)} \quad \text{(S5a)}$$

Where $\chi^{S=2}$ is the trace of the rotation matrix by an angle ϕ, and S the spin quantum number (here S=2). The representation of the S = 2 spin function may thus be decomposed into the following sum of irreducible representations:

$$\Gamma^{S=2} = A_1 + B_1 + B_2 + E \quad \text{(S5b)}$$

The configuration $^5A_{1g}$ (in the D_{4h} point group) is fully symmetric. Hence it is A_1 in the D_4 double group. Therefore, the magnetic sublevels of the $^5A_{1g}$ wavefunction are decomposed into the following representation:

$$\Gamma = \Gamma^{S=2} \otimes A_1 = A_1 + B_1 + B_2 + E \quad \text{(S5c)}$$

The coupling of the symmetry-adapted states is shown in Figure S5.

The effect of including the $^5A_{1g}$ state in the model is marginal (Figure S5). Despite slightly reducing the magnetic susceptibility at low temperatures, inclusion of the quintet state does not have a significant effect on the magnetic susceptibility at high temperature.

The low-temperature changes may all be explained by the increase of zero-field splitting axial parameter (114 cm^{-1}) compared to the value found without including the $^5A_{1g}$ (94 cm^{-1}). The increase of the zero-field splitting axial parameter reduces the Zeeman couplings between ground and excited magnetic sublevels, hereby reducing the magnetic moment of the ground sublevel in the *xy* plane. Since the ground magnetic sublevel is the only significantly populated sublevel at low temperature, this effect entirely explains the slight decrease of low-temperature magnetic susceptibility arising from inclusion of the $^5A_{1g}$ into the model.

On the other hand, the high-temperature susceptibility is only marginally affected by the inclusion of the $^5A_{1g}$ state, because the average *g*-value remains almost identical. Using Chibotaru's method (see below), we indeed found that the average g-value is 2.72, i.e. only 0.01 higher than the average value calculated without including the quintet state. The transverese *g*-value ($g_\perp$) is 3.06, which is almost identical to that found without inclusion of the $^5A_{1g}$ state (3.05). In details, however, the orbital contribution ($g_{L,\perp}$) decreases significantly

compared to the value calculated without including the $^5A_{1g}$, but this downshift is compensated by a similar upshift of the spin contribution ($g_{S,\perp}$). Similarly, the longitudinal g-value ($g_{\parallel}$) is almost unaffected by the inclusion of the quintet state (1.87 and 1.85 with and without inclusion of $^5A_{1g}$, respectively). However, behind this apparent constancy hides a slight upshift of the spin contribution ($g_{S,\parallel}$) compensated by a slight downshift of the orbital contribution ($g_{L,\parallel}$) (Table S2).

Table S2: Effect of the inclusion of the quintet state $^5A_{1g}$ in the effective Hamiltonian on the *g*-values of **1**. g_L and g_S correspond to the orbital and spin components of the *g*-values, respectively.

	$g_{\perp}$ ($g_{L,\perp}$/ $g_{S,\perp}$)	$g_{\parallel}$ ($g_{L,\parallel}$/ $g_{S,\parallel}$)	g_{av}
Not including $^5A_{1g}$	3.05 (1.14/1.91)	1.85 (0.08/1.77)	2.71
Including $^5A_{1g}$	3.06 (0.95/2.11)	1.87 (0.06/1.81)	2.72

In general, including the quintet state increases the g_S values and decreases the g_L values. The former phenomenon is readily explained by the mixing of $S = 2$ character into the $S = 1$ magnetic triplet. The latter phenomenon is more indirect. The mixing of the quintet state into the magnetic triplet decreases the $^3A_{2g}$ and $^3E_g^{\theta}$ components that are responsible for the large orbital angular momentum in the system. On the other hand, there is no first-order orbital momentum in $^5A_{1g}$. Likewise, there is no orbital Zeeman coupling element between the $^5A_{1g}$ and $^3E_g^{\theta}$ or $^3A_{2g}$ to induce additional orbital angular momentum under an applied field. Hence the mixing of the $^5A_{1g}$ state into the ground triplet only decrease its total orbital angular momentum. These findings thus showed that the inclusion of $^5A_{1g}$ have negligible effect on the overall magnetic properties of the system. Perhaps more importantly, it should be emphasized that the inclusion of the $^5A_{1g}$ state cannot explain the large orbital angular momentum of this system, which constitutes one of its main features. Hence, we do not consider it further.

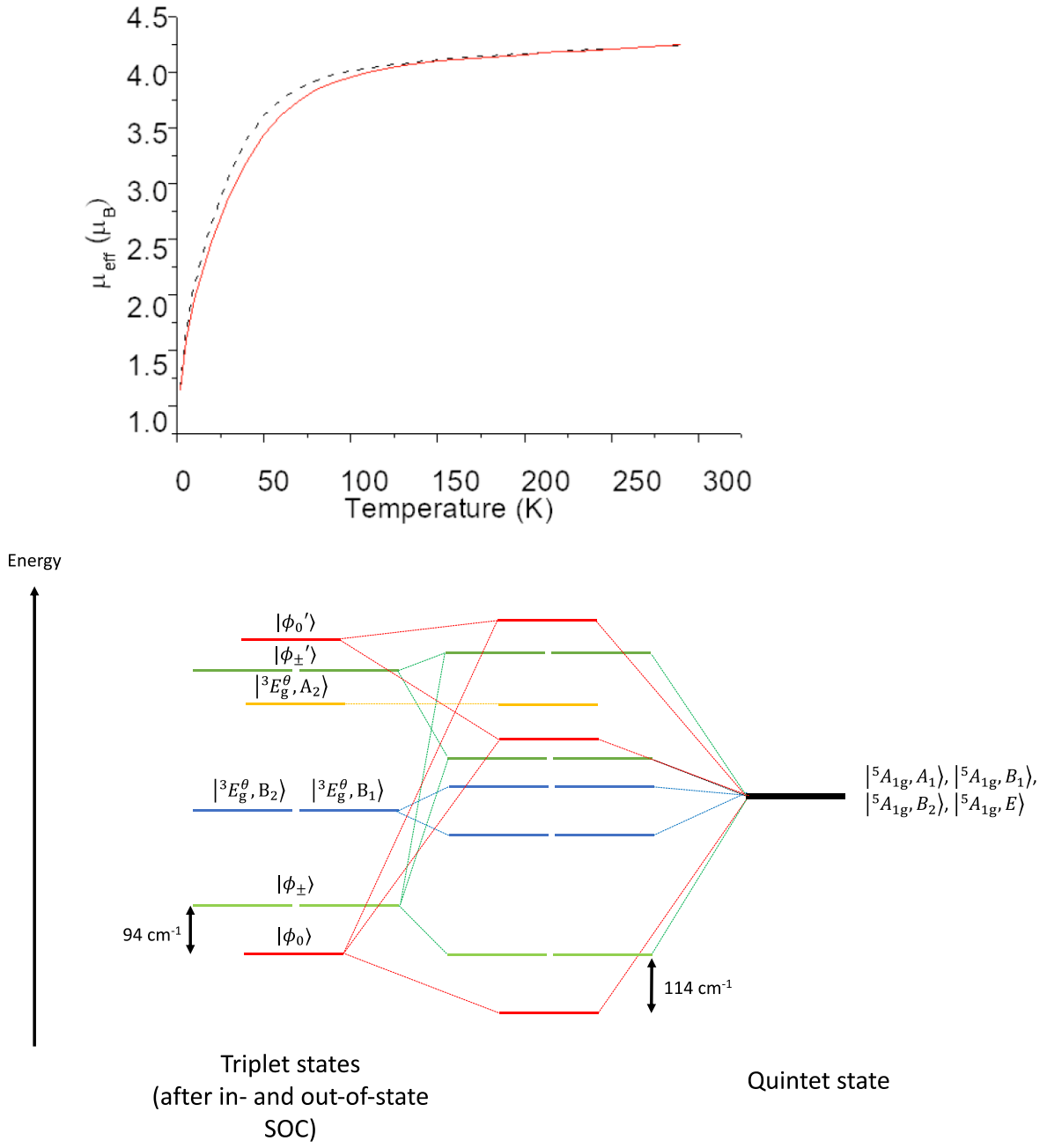

Figure S5: (Top) effect of the inclusion in the effective Hamiltonian of the $^5A_{1g}$ state 800 cm^{-1} above the $^3A_{2g}$ state on the effective magnetic moment. The red line and the black dashed line correspond to the effective magnetic moment of **1** with and without the $^5A_{1g}$ state included in the model, respectively. (Bottom) energy diagram showing the magnetic sublevels resulting from the SOC between (1) the magnetic sublevels arising from the SOC between the $^3A_{2g}$ and $^3E_g^\theta$ states (left-hand side) and the magnetic sublevels of the $^5A_{1g}$ orbital state (right-hand side). The color code represents the representation of the sublevels in the D_4 point group. E states are shown in green, B_1 and B_2 states are shown in blue, and the A_1 state are shown in red. The A_2 state is shown in orange.

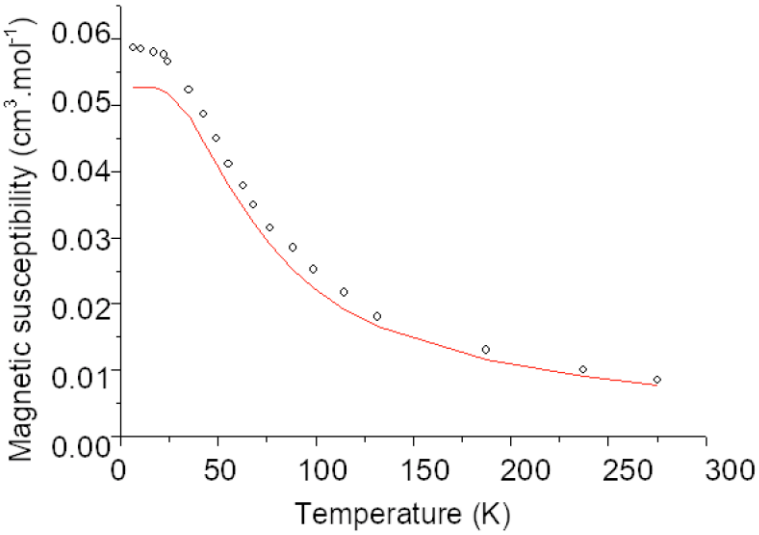

Figure S6: magnetic anisotropy of **1**, taken as $\chi_{\perp} - \chi_{\parallel}$, calculated using the effective Hamiltonian with the following parameters (see Main text): $\Delta_{A-E} = 950$ cm^{-1}, $\theta = -0.13\pi$. The solid red line represents the fit, and the dots represent the experimental measurements as taken from ref. 11.

Extraction of the spin Hamiltonian parameters

The magnetic sublevels $|\phi_+\rangle$, $|\phi_-\rangle$ and $|\phi_0\rangle$ constitute the space in which the electronic Zeeman and hyperfine coupling operators are expressed (if second-order Zeeman effects with higher-lying states are neglected, see main text). In parallel, the fictitious pseudo-spin eigenstates $|\tilde{S}=1, M_{\tilde{S}}=+1\rangle$, $|\tilde{S}=1, M_{\tilde{S}}=-1\rangle$ and $|\tilde{S}=1, M_{\tilde{S}}=0\rangle$ constitute the space in which the spin Hamiltonian Zeeman and hyperfine coupling operators are expressed. The extraction method consists in finding the spin Hamiltonian parameters such as the matrix elements of the electronic operators are one-by-one equivalent to their spin Hamiltonian counterpart.

We will not derive a general method to extract spin Hamiltonian parameters, which has been published by Chibotaru and coworkers.[12] Instead, we attach to obtain simple expressions for the *g*- and *A*-values in this specific system. Because of the high C_4 symmetry axis of the system, the *g*- and *A*- matrices must be already diagonal in the chosen molecular framework (i.e. the *xy* plane corresponds to the plane of the porphyrin ligand), and the x- and y- components in both these matrices must be identical. This considerably simplify our task as the total number of independent spin Hamiltonian parameters must be equal to 4 ($g_\perp$, $A_\perp$, $g_\parallel$, and $A_\parallel$). The magnetic moment parameters ($g_\perp$ and $g_\parallel$) will be extracted first. A similar demonstration may then be done to extract the hyperfine field parameters ($A_\perp$and $A_\parallel$).

First, using time-reversal symmetry arguments, we identify the independent matrix elements required to describe the effective Hamiltonian magnetic moment matrices. Second, we identify the independent matrix elements required in order to describe the spin Hamiltonian magnetic moment matrices. Then, we establish all the independent relationships between spin Hamiltonian and effective Hamiltonian matrix elements that need to be fulfilled in order to have a one-by-one equivalency between both matrices. Finally, we extract the spin Hamiltonian parameters by using the established relationship as a requirement.

In the basis of $|\phi_+\rangle$, $|\phi_-\rangle$ and $|\phi_0\rangle$, the μ_x, μ_y and μ_z components of the magnetic moment vector are each described by a 3x3 Hermitian matrix. Each of these matrices has 6 *a priori* independent matrix elements. Three of these six matrix elements are off-diagonal and need to be described with two independent parameters which potentially have a real and imaginary part. This adds up to a total of 18 matrix elements and 27 parameters to describe the three magnetic moment matrices. Because $|\phi_+\rangle$, $|\phi_-\rangle$ have opposite first-order angular momenta and $|\phi_0\rangle$ has no first-order angular momentum, we can make use of time-reversal symmetry to establish relationships between matrix elements and hence reduce the number of

independent parameters necessary to describe the magnetic moment matrices. Indeed, let there be a state with a first-order angular momentum, for which:

$$\hat{\theta}|\phi_+^{TR}\rangle = \langle\phi_-^{TR}| \quad \text{(S6a)}$$

Where $\hat{\theta}$ is the time-reversal operator. And let there be a state without first-order angular momentum,

$$\hat{\theta}|\phi_0^{TR}\rangle = \langle\phi_0^{TR}| \quad \text{(S6b)}$$

Since the states $|\phi_+\rangle$, $|\phi_-\rangle$ and $|\phi_0\rangle$ have undefined phase factors, they relate to the states $\left|\phi_\pm^{TR}\right\rangle$, $|\phi_0^{TR}\rangle$ by the following relationship

$$|\phi_0\rangle = e^{i\Theta_0}|\phi_0^{TR}\rangle \quad \text{(S6c)}$$

$$\left|\phi_\pm\right\rangle = e^{i\Theta_\pm}\left|\phi_\pm^{TR}\right\rangle \quad \text{(S6d)}$$

Where Θ_0, $\Theta_\pm$ are the respective phase angles.

and because the magnetic moment operator is time-odd, we have the following equalities:

$$\langle\phi_+|\mu_\alpha|\phi_+\rangle = \langle\theta\phi_-|\mu_\alpha|\theta\phi_-\rangle = \langle\phi_-|\theta^\dagger\mu_\alpha\theta|\phi_-\rangle = -\langle\phi_-|\mu_\alpha|\phi_-\rangle \quad \text{(S7a)}$$

$$\langle\phi_0|\mu_\alpha|\phi_0\rangle = \langle\theta\phi_0|\mu_\alpha|\theta\phi_0\rangle = -\langle\phi_0|\mu_\alpha|\phi_0\rangle = 0 \quad \text{(S7b)}$$

$$\langle\phi_-|\mu_\alpha|\phi_+\rangle = e^{i(\Theta_+-\Theta_-)}\langle\phi_-^{TR}|\mu_\alpha|\phi_+^{TR}\rangle = e^{i(\Theta_+-\Theta_-)}\langle\theta\phi_-^{TR}|\mu_\alpha|\theta\phi_+^{TR}\rangle$$
$$= -e^{i(\Theta_+-\Theta_-)}\langle\phi_-^{TR}|\mu_\alpha|\phi_+^{TR}\rangle = -\langle\phi_-|\overrightarrow{\mu_\alpha}|\phi_+\rangle \quad \text{(S7c)}$$

Obviously, relationship (S7c) becomes:

$$\langle\phi_-|\overrightarrow{\mu_\alpha}|\phi_+\rangle = 0 \quad \text{(S7d)}$$

Finally,

$$\langle\phi_0|\overrightarrow{\mu_\alpha}|\phi_+\rangle = e^{i(\Theta_+-\Theta_0)}\langle\phi_0^{TR}|\overrightarrow{\mu_\alpha}|\phi_+^{TR}\rangle = e^{i(\Theta_+-\Theta_0)}\langle\phi_-^{TR}|\theta^\dagger\overrightarrow{\mu_\alpha}\theta|\phi_0^{TR}\rangle$$
$$= -e^{i(\Theta_+ + \Theta_- - 2\Theta_0)}\langle\phi_-|\overrightarrow{\mu_\alpha}|\phi_0\rangle \quad \text{(S7e)}$$

Similarly, the phase factor $= e^{i(\Theta_+ + \Theta_- - 2\Theta_0)}$ is undefined and may be taken so that:

$$\langle\phi_0|\overrightarrow{\mu_\alpha}|\phi_+\rangle = \langle\phi_-|\overrightarrow{\mu_\alpha}|\phi_0\rangle \quad \text{(S7f)}$$

It can be verified that S7f is respected for the chosen phase factors in the description of $|\phi_0\rangle$, $|\phi_\pm\rangle$ (Eq. 8a and 8b in the Main Text). Taking those relationships into accounts greatly decreases the number of independent matrix elements down to one diagonal and one off-diagonal for each matrix, i.e. a total of 6 matrix elements, i.e. $\langle\phi_+|\mu_x|\phi_+\rangle$, $\langle\phi_+|\mu_y|\phi_+\rangle$, $\langle\phi_+|\mu_z|\phi_+\rangle$, $\langle\phi_0|\mu_x|\phi_+\rangle$, $\langle\phi_0|\mu_y|\phi_+\rangle$, $\langle\phi_0|\mu_y|\phi_+\rangle$ (9 parameters).

It is trivial to show with ladder operator techniques that the spin Hamiltonian magnetic moment matrices in the basis $|\tilde{S}=1, M_{\tilde{S}}\rangle$ follow the exact same constraints. Specifically, the pseudospin eigenstates $|\tilde{S}, M_{\tilde{S}}\rangle$ have the same time-reversal properties as the $|\phi_+\rangle$, $|\phi_-\rangle$ and $|\phi_0\rangle$ states, i.e.

$$\langle \tilde{\mathrm{S}} = 1, \mathrm{M}_{\tilde{S}} = +1 | \mu_\alpha^{SH} | \tilde{\mathrm{S}} = 1, \mathrm{M}_{\tilde{S}} = +1 \rangle = -\langle \tilde{\mathrm{S}} = 1, \mathrm{M}_{\tilde{S}} = -1 | \mu_\alpha^{SH} | \tilde{\mathrm{S}} = 1, \mathrm{M}_{\tilde{S}} = -1 \rangle \quad \text{(S8a)}$$

$$\langle \tilde{\mathrm{S}} = 1, \mathrm{M}_{\tilde{S}} = 0 | \mu_\alpha^{SH} | \tilde{\mathrm{S}} = 1, \mathrm{M}_{\tilde{S}} = 0 \rangle = 0 \quad \text{(S8b)}$$

$$\langle \tilde{\mathrm{S}} = 1, \mathrm{M}_{\tilde{S}} = +1 | \mu_\alpha^{SH} | \tilde{\mathrm{S}} = 1, \mathrm{M}_{\tilde{S}} = -1 \rangle = 0 \quad \text{(S8c)}$$

$$\langle \tilde{\mathrm{S}} = 1, \mathrm{M}_{\tilde{S}} = 0 | \mu_\alpha^{SH} | \tilde{\mathrm{S}} = 1, \mathrm{M}_{\tilde{S}} = +1 \rangle = \langle \tilde{\mathrm{S}} = 1, \mathrm{M}_{\tilde{S}} = -1 | \mu_\alpha^{SH} | \tilde{\mathrm{S}} = 1, \mathrm{M}_{\tilde{S}} = 0 \rangle \quad \text{(S8d)}$$

Where μ_α^{SH} is the α- component of the magnetic moment operator described in the spin Hamiltonian formalism (see Eq. S1). Those relationships make the number of independent matrix elements decrease down to 6 (9 parameters), i.e.

$$\langle \tilde{\mathrm{S}} = 1, \mathrm{M}_{\tilde{S}} = +1 | \mu_x^{SH} | \tilde{\mathrm{S}} = 1, \mathrm{M}_{\tilde{S}} = +1 \rangle = g_{xz} \quad \text{(S9a)}$$

$$\langle \tilde{\mathrm{S}} = 1, \mathrm{M}_{\tilde{S}} = +1 | \mu_y^{SH} | \tilde{\mathrm{S}} = 1, \mathrm{M}_{\tilde{S}} = +1 \rangle = g_{yz} \quad \text{(S9b)}$$

$$\langle \tilde{\mathrm{S}} = 1, \mathrm{M}_{\tilde{S}} = +1 | \mu_z^{SH} | \tilde{\mathrm{S}} = 1, \mathrm{M}_{\tilde{S}} = +1 \rangle = g_{zz} \quad \text{(S9c)}$$

$$\langle \tilde{\mathrm{S}} = 1, \mathrm{M}_{\tilde{S}} = 0 | \mu_x^{SH} | \tilde{\mathrm{S}} = 1, \mathrm{M}_{\tilde{S}} = +1 \rangle = \frac{g_{xx} + i g_{xy}}{\sqrt{2}} \quad \text{(S9d)}$$

$$\langle \tilde{\mathrm{S}} = 1, \mathrm{M}_{\tilde{S}} = 0 | \mu_y^{SH} | \tilde{\mathrm{S}} = 1, \mathrm{M}_{\tilde{S}} = +1 \rangle = \frac{g_{yx} + i g_{yy}}{\sqrt{2}} \quad \text{(S9e)}$$

$$\langle \tilde{\mathrm{S}} = 1, \mathrm{M}_{\tilde{S}} = 0 | \mu_z^{SH} | \tilde{\mathrm{S}} = 1, \mathrm{M}_{\tilde{S}} = +1 \rangle = \frac{g_{zx} + i g_{zy}}{\sqrt{2}} \quad \text{(S9f)}$$

Hence, the spin Hamiltonian and effective Hamiltonian magnetic moment matrices are equivalent under the following conditions:

$$\langle \phi_+ | \mu_\alpha | \phi_+ \rangle = \langle \tilde{S} = 1, \mathrm{M}_{\tilde{S}} = +1 | \mu_\alpha^{SH} | \tilde{S} = 1, \mathrm{M}_{\tilde{S}} = +1 \rangle \quad \text{(S10a)}$$

$$\langle \phi_0 | \mu_\alpha | \phi_+ \rangle = \langle \tilde{\mathrm{S}} = 1, \mathrm{M}_{\tilde{S}} = 0 | \mu_\alpha^{SH} | \tilde{\mathrm{S}} = 1, \mathrm{M}_{\tilde{S}} = +1 \rangle \quad \text{(S10b)}$$

Those relationships enable the expression of the g-values in terms of the effective Hamiltonian magnetic moment matrix elements, which are known from our effective Hamiltonian analysis. We immediately find that the g-matrix is diagonal, i.e. $g_{xz} = g_{zx} = g_{xy} = g_{yx} = g_{yz} = g_{zy} = 0$, which confirms that the molecular framework is colinear the proper axes of the g-matrix, consistently with the high symmetry of the molecule. The diagonal values may be expressed in terms of the effective Hamiltonian magnetic moment matrix elements, i.e.:

$$|g_{\mathrm{zz}}| = |\langle \phi_+ | \overrightarrow{\mu_z} | \phi_+ \rangle| \quad \text{(S11a)}$$

$$|g_{xx}| = \sqrt{2} |\langle \phi_0 | \overrightarrow{\mu_x} | \phi_+ \rangle| \quad \text{(S11b)}$$

$$|g_{yy}| = \sqrt{2} |i \langle \phi_0 | \overrightarrow{\mu_y} | \phi_+ \rangle|. \quad \text{(S11c)}$$

It is verified that $|g_{xx}| = |g_{yy}| = |g_\perp|$ (the sign of the g-values was not investigated and arbitrarily set positive for simplicity).

Eq. S11 correspond to the extracted g-values shown in the main text. This demonstration is heavily inspired by Chibotaru's method, but is adapted for this specific case. Rather than

building the Abragam-Bleaney tensor, it makes use of symmetry arguments to establish a simple relationship between *g*-values and matrix elements.

The procedure used to extract the *A* values is completely equivalent to the demonstration above. One simply replaces the magnetic moment matrices with the hyperfine field matrices. In total analogy, one finds that $A_{xz} = A_{zx} = A_{xy} = A_{yx} = A_{yz} = A_{zy} = 0$.

For the diagonal values,

$$\frac{A_{\perp}}{g_N \beta_N} = \sqrt{2}\left|\langle \phi_0 | \overrightarrow{B_{int,x}} | \phi_+ \rangle\right| \quad \text{(S12a)}$$

$$\frac{A_{zz}}{g_N \beta_N} = \left|\langle \phi_+ | \overrightarrow{B_{int,z}} | \phi_+ \rangle\right| \quad \text{(S12b)}$$

Eq. S12a and S12b correspond to the extracted *A*-values shown in the main text. In principle, the three *A* values appear from this treatment with a sign that is consistent with the sign of *g*. In our case, since we arbitrarily set the sign of all *g*-values to be positive, we instead calculated the absolute value of A and then chose the sign to be consistent with the experimental direction of the internal field.

Discussion on the corrections to the microscopic magnetic moments

The microscopic magnetic moments are underestimated in spin Hamiltonian formalism, due to the neglection of the second-order Zeeman effects with excited magnetic sublevels (see Main Text). A state-specific correction accounting for these second-order couplings must be applied to recover the magnetic moment calculated with the developed effective Hamiltonian. This correction may be estimated using second-order perturbation theory. Indeed, due to Hellmann-Feynman theorem,

$$\langle \mu_\alpha \rangle = -\left\langle \frac{d\widehat{H_{Zee}}}{dB_\alpha} \right\rangle = -\frac{dE}{dB_\alpha} \quad \text{(S13)}$$

Where $\widehat{H_{Zee}}$ is defined according to Eq. 4c in the main text. The B_α correspond to the components of the applied field. So, in the framework of second-order perturbation theory, for instance for $|\widetilde{\phi_0}\rangle$,

$$\langle \mu_\alpha \rangle_0 = \langle \widetilde{\phi_0} | \mu_\alpha | \widetilde{\phi_0} \rangle - \sum_\beta B_\beta \sum_i \frac{\langle \widetilde{\phi_0} | \mu_\alpha | \psi_i \rangle \langle \psi_i | \mu_\beta | \widetilde{\phi_0} \rangle + \langle \widetilde{\phi_0} | \mu_\beta | \psi_i \rangle \langle \psi_i | \mu_\alpha | \widetilde{\phi_0} \rangle}{\epsilon_0 - \epsilon_i} \quad \text{(S14)}$$

It is assumed here that the $|\widetilde{\phi_0}\rangle$, $|\widetilde{\phi_\pm}\rangle$ are eigenstates of the Hamiltonian in the basis of $|\phi_0\rangle$, $|\phi_\pm\rangle$ for a given applied field. The ψ_i correspond to the excited magnetic sublevels (higher than $|\widetilde{\phi_\pm}\rangle$) with energies ϵ_i. ϵ_0 corresponds to the energy of the magnetic state $|\widetilde{\phi_0}\rangle$. As usual, the α and β components represent the x, y or z-components.

Thus, the first term in Eq. S14 corresponds to the spin Hamiltonian value of μ_α (assuming the spin Hamiltonian parameters have been calculated with the method described above), and the second correspond to the corrections due to second-order Zeeman effects with excited magnetic sublevels. It is apparent that these corrections are state-specific because each magnetic sublevel interacts with distinct excited sublevels. Hence, the sublevel $|\phi_0\rangle$ interacts with the sublevel $|\phi'_\pm\rangle$ (Figure 8 in Main text) from which it is separated by about 1333 cm^{-1}, while the sublevels $|\phi_\pm\rangle$ mainly interact with the sublevels $|^3E_g, B_1\rangle$ and $|^3E_g, B_2\rangle$, from which they are separated by only 957 cm^{-1}. Consequently, the correction for the $|\phi_\pm\rangle$ sublevels are more important than for $|\phi_0\rangle$ (table 6 in the main text, Eq. S14). Finally, the corrections to the spin and orbital momenta are linear with the external field, as predicted by second-order perturbation theory (see Eq. S14).

In detail, these corrections mainly arise from the transverse orbital Zeeman effect, owing to the fact that the ground triplet, even after spin-orbit coupling, is still dominated by the $^3A_{2g}$ electronic configuration (85-88%), while the excited state is dominated by $^3E_g^\theta$.

Consequently, the corrections are anisotropic, because $^3A_{2g}$ only interacts with $^3E_g^\theta$ through the *xy* component of the orbital moment operator.

In principle, the magnetic correction being state-specific, the correction of the magnetic susceptibility must be temperature-dependent since it depends on the relative population of the magnetic sublevels. This correction term can be approximated to the following expression:

$$\Delta\chi = \frac{2}{3B_{ext}} N \frac{\sum_i (\mu_{i,\perp}^{EH} - \mu_{i,\perp}^{SH}) e^{-\frac{E_i}{k_B T}}}{\sum_i e^{-\frac{E_i}{k_B T}}} \quad \text{(S15)}$$

Where the factor $\frac{2}{3}$ accounts for the powder-averaging of the correction (only the transverse magnetic moments deviates significantly from the spin Hamiltonian value), N is the Avogadro number, $\mu_{i,\perp}^{EH}$ and $\mu_{i,\perp}^{SH}$ are the transverse magnetic moments of the sublevels i described with the spin Hamiltonian and effective Hamiltonian, respectively (Table 6 in the Main Text), E_i the energy of the sublevel i. As usual, k_B is the Boltzmann constant and T is the temperature.

However, this correction can be approached with a standard TIP correction for two reasons: (1) the magnetic moments corrections are similar, if not identical, for each magnetic sublevel of the triplet (Table 6), and (2) for effective magnetic moments measurements, the correction only becomes visible at high temperatures (>100 K) where the population of the three sublevels is close to being equalized (Figure S7).

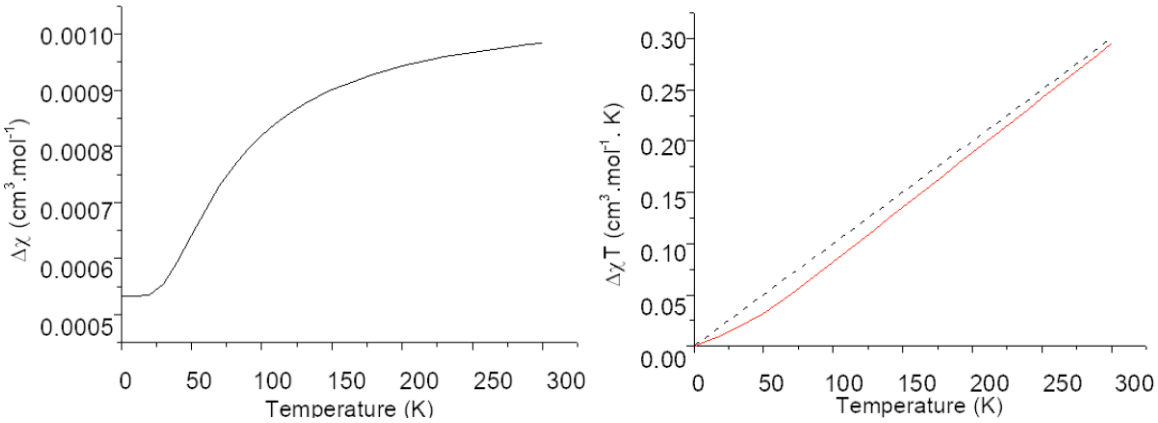

Figure S7: (left) thermal average of the magnetic susceptibility correction, and (right) corresponding thermal average of $\Delta\chi T$ (red line) under a field of 1 T. For comparison, the phenomenological TIP $\Delta\chi = 1000 \times 10^{-6}$ emu is represented by the dashed black line.

References

(1) Rawlings, D. C.; Gouterman, M., Theoretical investigations of the electronic states of porhyrins. III. Low-lying electronic states of porphinatoiron(II). *Int. J. Quantum Chem.*, **1985**, *28*, 773-796

(2) Manni, G. L.; Alavi, A., Understanding the mechanism stabilizing intermediate spin states in Fe(II)-porphyrin. *J. Phys. Chem. A*, **2018**, *122*, *22*, 4935-4947

(3) (a) Choe, Y-K.; Hashimoto, T.; Nakano, H.; Hirao, K., Theoretical study of the electronic ground state of iron(II) porphine. *Chem. Phys. Lett.*, 1998, 295, 380-388.

(4) Choe, Y. K.; Nakajima, T.; Hirao, K.; Lindh, R., Theoretical study of the ground state of the electronic ground state of iron(II) porphine II. *J. Chem. Phys.*, 1999, 111, 3837.

(5) Pierloot, K.; Phung, Q. M.; Domingo, A., Spin state energetics in First-Row Transition Metal Complexes: Contribution of (3s3p) correlation and its description by second-order perturbation theory. *J. Chem. Theory Comput.*, **2017**, *13*, 537−553.

(6) Radon, M., Spin-state energetics of heme-related models from DFT and coupled-cluster calculations. *J. Chem. Theory Comput*., 2014, 10, 2306−2321.

(7) Altun, A.; Saitow, Masaaki ; Neese, F.; Bistoni, G., Local energy decomposition of open-shell molecular systems in the domain-based local pair natural orbital coupled cluster framework. *J. Chem. Theory Comput.*, **2019**, *15*, 1616-1632

(8) (a) Nehrkorn, J.; Holldack, K.; Bittl, R.; Schnegg, A. Recent Progress in Synchrotron-Based Frequency-Domain Fourier-Transform THz-EPR. *J. Magn. Reson.* **2017**, *280*, 10–19. (b) Nehrkorn, J.; Martins, B. M.; Holldack, K.; Stoll, S.; Dobbek, H.; Bittl, R.; Schnegg, A. Zero-Field Splittings in MetHb and MetMb with Aquo and Fluoro Ligands: A FD-FT THz-EPR Study. *Mol. Phys.* **2013**, *111*, 2696–2707. (c) Schnegg, A.; Behrends, J.; Lips, K.; Bittl, R.; Holldack, K. Frequency Domain Fourier Transform THz-EPR on Single Molecule Magnets Using Coherent Synchrotron Radiation. *Phys. Chem. Chem. Phys.* **2009**, *11*, 6820-6825.

(9) Stoll, S.; Schweiger, A. EasySpin, a Comprehensive Software Package for Spectral Simulation and Analysis in EPR. *J. Magn. Reson.* **2006**, *178*, 42–55.

(10) (a) Nehrkorn, J.; Schnegg, A.; Holldack, K.; Stoll, S. General Magnetic Transition Dipole Moments for Electron Paramagnetic Resonance. *Phys. Rev. Lett.* **2015**, *114*, 010801. (b) Nehrkorn, J.; Telser, J.; Holldack, K.; Stoll, S.; Schnegg, A. Simulating Frequency-Domain Electron Paramagnetic Resonance: Bridging the Gap between Experiment and Magnetic

Parameters for High-Spin Transition-Metal Ion Complexes. *J. Phys. Chem. B* **2015**, *119*, 13816–13824.

(11) Boyd, P. D. W.; Buckingham, D. A.; McMeeking, R. F.; Mitra, S., Paramagnetic anisotropy, average magnetic susceptibility, and electronic structure of intermediate-spin S = 1 (5,10,15,10-tetraphenylporphyrin)iron(II), *Inorg. Chem.*, **1979**, *18*, 3585-3591.

(12) Chibotaru, L. F.; Ungur, L., Ab-initio calculation of anisotropic magnetic properties of complexes. I. Unique definition of pseudospin Hamiltonians and their derivation, *J. Chem. Phys*., **2012**, *137*, 064112